Proceedings of ASME Turbo Expo 2010: Power for Land, Sea and Air
GT2010
June 14-18, 2010, Glasgow, UK

GT2010-22964

CFD ANALYSIS OF FLOW AND HEAT TRANSFER IN A DIRECT TRANSFER PRE-SWIRL SYSTEM

Umesh Javiya
u.javiya@surrey.ac.uk

John Chew
j.chew@surrey.ac.uk

Nick Hills
n.hills@surrey.ac.uk

Fluid Research Centre
Faculty of Engineering and Physical Science
University of Surrey
Guildford, Surrey, GU2 7XH, UK

Leisheng Zhou*
lz242@bath.ac.uk

Mike Wilson
m.wilson@bath.ac.uk

Gary Lock
g.d.lock@bath.ac.uk

Department of Mechanical Engineering
University of Bath
Bath, BA2 7AY, UK

ABSTRACT

The accuracy of computational fluid dynamics (CFD) for the prediction of flow and heat transfer in a direct transfer pre-swirl system is assessed through a comparison of CFD results with experimental measurements. Axisymmetric and three dimensional (3D) sector CFD models are considered. In the 3D sector models, the pre-swirl nozzles or receiver holes are represented as axisymmetric slots so that steady state solutions can be assumed. A number of commonly used turbulence models are tested in three different CFD codes, which were able to capture all of the significant features of the experiments. Reasonable quantitative agreement with experimental data for static pressure, total pressure and disc heat transfer is found for the different models, but all models gave results which differ from the experimental data in some respect. The more detailed 3D geometry did not significantly improve the comparison with experiment, which suggested deficiencies in the turbulence modelling, particularly in the complex mixing region near the pre-swirl nozzle jets. The predicted heat transfer near the receiver holes was also shown to be sensitive to near-wall turbulence modelling. Overall, the results are encouraging for the careful use of CFD in pre-swirl-system design.

*Present address at school of power and energy engineering, Northwestern Polytechnic University, Xi'an, China.

NOMENCLATURE

a	rotor inner radius, m
b	rotor outer radius, m
C_m	angular moment coefficient ($=M/0.5\rho\Omega^2 b^5$)
C_p	specific heat capacity at constant pressure, J/kgK
C_w	non-dimensional mass flow rate ($=\dot{m}/\mu b$)
D	moment on the stator walls, Nm
d_h	receiver hole diameter, m
d_p	nozzle diameter, m
h	heat transfer coefficient, W/m^{2}K
k_a	thermal conductivity for air, (W/mK)
k	turbulence kinetic energy, m^2/s^2
K	swirl fraction, ($= v_\phi/\Omega r$)
l_h	receiver hole length, m
l_p	pre-swirl nozzle length, m
$\dot{m}$	mass flow rate, kg/s
M	moment on the rotor walls, Nm
N_h	number of receiver holes
N_p	number of pre-swirl nozzles
Nu	Nusselt number ($=hr/k_a$)
p	static pressure, N/m^2
P_o	gauge Total pressure, N/m^2

Pr	Prandlt number, (= $C_p\mu/k_a$)
q_w	wall heat flux W/m^2
Q	heat transfer to the system, W
r	radius, m
r_h	receiver hole radial location, m
r_p	nozzle radial location, m
Re_ϕ	rotational Reynolds number, (= $\rho\Omega b^2/\mu$)
s	pre-swirl chamber width, m
SR_p	nozzle exit or chamber inlet swirl ratio, (= $v_{\phi,p}/\Omega r_p$)
T_o	total temperature, K
T	temperature, K
u_τ	friction velocity
v	velocity, m/s
v_ϕ	swirl/tangential velocity, m/s
$v_{\phi,p}$	swirl velocity at nozzle exit, m/s
$\dot{W}$	work transfer to the system, W
y	distance normal to the wall
y^+	nondimensional wall distance (= $\rho y u_\tau/\mu$)
ε	turbulence dissipation rate, m^2/s^3
ρ	density of air, kg/m^3
λ_T	mass flow-rate parameter (= $C_w\mathrm{Re}_\phi^{-0.8}$)
μ	molecular viscosity of air, Ns/m^2
ω	Specific dissipation rate, s^{-1}
Ω	rotation speed of the rotor disc, rad/s

Subscript

Ad	Adiabatic
isen	Isentropic
O	total value in stationary frame
P	pre-swirl
R	at radial location *r*
s	Stator
bl	boundary-layer
w	rotor wall
ϕ,r,z	circumferential, radial and axial coordinates

1 INTRODUCTION

In gas turbines, air is diverted from the compressor through a secondary air system, which supplies cooling air to the turbine components and prevents hot-gas ingestion from the main annulus into the turbine disc cavities. In a high-pressure turbine stage, this cooling air is expanded through stationary, angled pre-swirl nozzles, transferred through a wheel-space, and delivered to blade receiver holes on the rotating disc. The nozzles swirl the air, and this reduces the work done by the rotating turbine disc in accelerating the air to the disc speed. This consequently reduces the relative total temperature of the air entering the receiver holes, which guide the coolant to the rotor-blade roots.

Pre-swirl research has been widely published at ASME conferences. Meierhofer and Franklin [1] were the first to publish experimental confirmation of the significant reduction in relative total temperature using a pre-swirl system, and quantified the effectiveness of such a system in terms of the ratio of delivery air velocity to disc speed. Recently, research work on pre-swirl systems has been advanced significantly by two major research programs funded by the European Commission on Internal Cooling Air Systems for Gas Turbines: ICAS-GT1 and ICAS-GT2 [2]. Most of the experimental work has been done at the University of Karlsruhe, using a direct-transfer system with the pre-swirl nozzles and receiver holes at nearly the same radius. Published experimental results for engine-representative geometries from these programs include measurements of discharge coefficient [3], use of particle image velocimetry [4], heat transfer measurements on the rotor disc [5] and evaluation of overall system performance in terms of measured delivery air temperature [6-7]. Computational analyses for these ICAS-GT programs have also been published [8-11]. Further experimental and numerical studies of pre-swirl systems are reported by the Universities of Sussex and Surrey [12-13] and the University of Bath [14-26].

Much of the published work focuses on cooling air delivery temperature and effectiveness assuming adiabatic systems. In an early study El-Oun and Owen [12] calculated delivery cooling air temperature and effectiveness with a simple theoretical model based on the Reynolds analogy. Chew *et al*. [13] presented a drag model based on an angular momentum balance for the stator-rotor system to calculate air delivery temperature and compared this with experimental data. Further improvement of this model and CFD results were given by Chew *et al*. [10]. The experimental data, elementary model and CFD indicated that the surface friction effects were quite small in their pre-swirl system. These and other studies indicate that reasonable estimates of air delivery temperature can be obtained from CFD, and that in many cases steady flow models give similar results to unsteady models. However, some uncertainties remain. These include heat transfer, which affects cooling air and disc temperatures, thereby influencing component life and running clearances.

The present study is motivated by the need to validate CFD for calculation of heat transfer in pre-swirl systems. A few previous studies of the heat transfer on the rotor disc have been published. These include experimental measurements by Bricaud *et al*. [5], Lock *et al*. [19] and Kakade *et al*. [20] for direct transfer systems, and by Wilson *et al*. [14] for a cover plate system. Bricaud *et al*. [5] estimated heat transfer from solution of the steady heat conduction equation for their rotor, with boundary temperatures supplied from thermocouple measurements. The other studies mentioned have used a transient experimental technique with thermochromic liquid crystals. CFD studies have been reported by Wilson *et al*. [14], Farzaneh-Gord *et al*. [17] and Lewis *et al*. [18], with some agreement with measurements.

In this paper CFD solutions are evaluated against both fluid flow and heat transfer measurements in a pre-swirl system, using various turbulence models and three different CFD codes. The pre-swirl configuration selected matches that studied

experimentally by Kakade *et al*. [20]. The experimental facility is briefly described in the next section, and the CFD models are described in section 3. For the axisymmetric case, various turbulence models are tested and compared with flow measurements in section 4.1 Three different 3D sector modelling approaches have been used and results from these models are compared with flow measurements in section 4.2. Heat transfer predictions are presented and compared with measurements in section 5. The main conclusions from this study are summarized in section 6.

2 EXPERIMENTAL DETAIL

Only key elements of the experimental details are given here. More details about the Bath experimental facility and methods can be found in Kakade *et al*. [22]. Experiments were conducted using a simplified model of a gas-turbine rotor-stator system. The geometry, which was based on information obtained for existing engine designs, is illustrated schematically in Figure 1. Air entered the test section through the stator at low radius via pre-swirl nozzles and flowed radially outward between the rotating disc and the stator, exiting through 60 axial receiver holes in the disc representing the entrance to blade-cooling passages in the engine. The air pressure in the wheel space was balanced by sealing air to restrict leakage or ingress. Kakade *et al.* [20] have used a very similar rotor system with the pre-swirl nozzles placed at same radius as the receiver holes ($r_p = r_h = 0.2$ m). The geometric properties of the test rig and the range of operating conditions are summarised in Table 1.

Disc outer radius, b	216 mm
Inner radius, a	$a/b = 0.67$
Gap ratio	$s/b = 0.051$
Pre-swirl radius, r_p	$r_h/b = 0.74$
Receiver-hole radius, r_h	$r_h/b = 0.93$
Receiver hole diameter, d_h	8 mm
l_h/d_h, for Receiver hole	1.25
Nozzle diameter, d_p	7.1 mm
l_p/d_p for pre-swirl nozzle	8.2
Re_ϕ	$0.78 \times 10^6 - 1.2 \times 10^6$
λ_T	0.125 – 0.36
SR_p	0.5 – 1.5
C_w	6600 – 27200

Table 1: Experimental geometry and operating conditions.

For turbulent pre-swirl flow in rotating cavities, where the gap ratio is large enough to ensure separate boundary layers, the swirling flow is expected to be governed principally by two non-dimensional variables: the inlet pre-swirl ratio, SR_p, and the mass flow rate parameter, $\lambda_T = C_w \mathrm{Re}_\phi^{-0.8}$. The fluid dynamics of this facility has been investigated both experimentally and computationally by Yan *et al.* [16]. The mass flow rates and disc rotational speed (typically 5000 rpm) were chosen to simulate engine-representative values of SR_p and λ_T and hence the flow structure is considered to be representative of that found in cooling systems of engines.

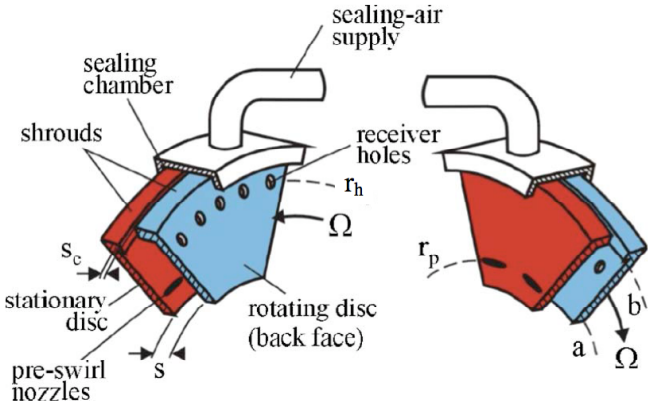

Fig. 1: Schematic diagram of test section [18].

Local heat transfer coefficients on the rotating disc were determined from transient surface temperature measurements using two calibrated narrow-band thermochromic liquid crystals (TLC). The experiments were conducted under known thermal boundary conditions, using air which had been pre-heated to ~60 C using the mesh heater upstream of the pre-swirl nozzles (see [19]). The method relied on the accurate measurement of the time taken for the crystals on the rotor surface to reach a unique value of hue, which had been accurately calibrated against temperature. The method of analysis to determine the heat transfer coefficient is described by Newton *et al.* [23] and Kakade *et al.* [24], and the experimental uncertainties, which include the effects of two-dimensional conduction, are described by Owen *et al.* [25] and Kingsley-Rowe *et al.* [26].

3 CFD MODELLING

Axisymmetric (2D) and three 3D sector models were created as shown in Figure 2. The dimensions are shown in Table 1. In all models, the sealing clearances between stator and rotor discs were neglected. For the axisymmetric model, both the nozzles and the receiver holes are represented as axisymmetric slots having the same total area as the corresponding nozzles or holes. Two of the 3D sector models (Figures 2c and 2d) represent the nozzles as an inlet slot, imposing inlet conditions either in the nozzle-exit plane or upstream of an extended slot geometry. Both models included the receiver holes and an exit plenum, and assumed steady flow in the rotating reference frame with circumferential periodicity on the 6° sector (corresponding to the 60 receiver holes used in the experiments). Checks were made to show that changing the plenum dimensions did not affect the pre-swirl chamber flow. The model in Figure 2e modelled the receiver holes as a slot, allowing a circumferentially periodic, steady solution in the stationary reference frame. The sector here is 15° corresponding to one of the 24 pre-swirl nozzles used in the experiments. Inlet conditions were applied to a plenum upstream of the nozzles, and exit conditions in the plane of the receiver-hole inlets.

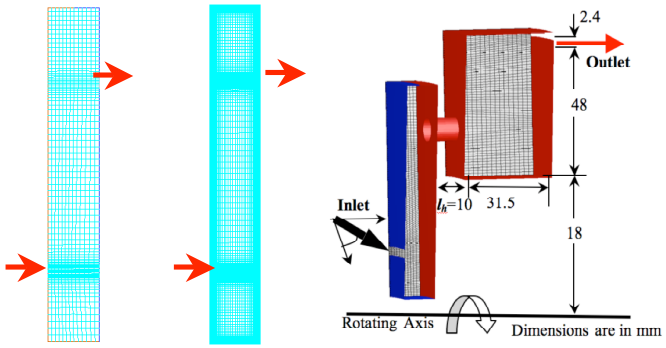

(a) 2D Coarse mesh **(b) 2D Fine mesh** **(c) 3D: with inlet slot**

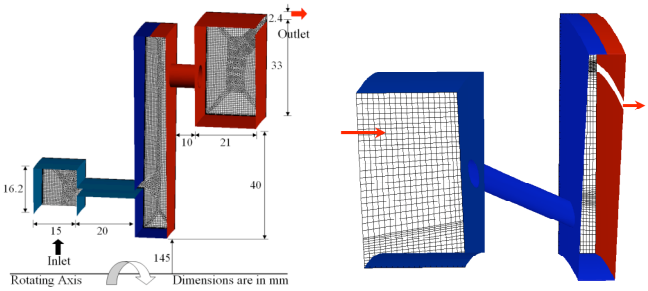

(d) 3D: extended inlet slot **(e) 3D: with nozzle**

Fig. 2: Model domains and meshes (■-Rotating and ■, ■-Stationary walls).

Two types of meshes were created depending on the near-wall turbulence modelling used: "coarse" meshes were generated for simulations that used wall functions and "fine" meshes for simulations that resolve the near wall flow. Examples are shown for the axisymmetric model in Figure 2. Careful consideration was given to the mesh near the walls, and mesh sensitivity studies were carried out to check that the results were not significantly dependent on the mesh size. The mesh sensitivity study showed that similar results were obtained for similar near-wall mesh y^+ values in corresponding codes. The different numerical treatments in different codes require different meshes to give similar y^+ values when using wall functions. Hence, when using the wall function, a similar range of y^+ values ($30 < y^+ < 100$) was used instead of the same mesh in different codes. When using resolved near-wall models where, the y^+ values were generally less than 1 and results were essentially mesh independent. Similar coarse and fine mesh approaches were adopted for both axisymmetric and 3D sector models. Meshes for FLUENT and Hydra consisted of hexahedral 3D elements or quadrilateral 2D elements. For the CFX computations, a hybrid mesh of prismatic and tetrahedral elements was used.

Solutions for the axisymmetric and inlet slot 3D cases were obtained in the rotating frame of reference. A stationary reference frame was used for the 3D model including the nozzle. Boundary conditions specifying the mass flow rate at the inlet and uniform static pressure at the outlet were applied. Inlet swirl was created on the models with slot inlets by

Model	Standard wall function models (with coarse mesh)	Near wall modelling	CFD code	Identifier
Axisymmetric	Standard k-ε	Wall functions	FLUENT	**F-2D-$k\varepsilon$-*WF***
	RNG (Renormalization group theory) k-ε			-
	Realizable k-ε			-
	Standard k-ω			-
	SST (Shear stress transport) k-ω			**F-2D-SST-*WF***
	Standard k-ε	Resolved wall treatment	FLUENT	**F-2D-$k\varepsilon$-*kl***
	SST k-ω			**F-2D-SST**
	Launder-Sharma's low Reynolds number (low Re) model			**F-2D-$k\varepsilon$-*LS***
3D with inlet slot	Standard k-ε model	Wall functions	FLUENT	**F-3DS-$k\varepsilon$- *WF***
		Resolved wall treatment	FLUENT	**F-3DS-$k\varepsilon$-*kl***
		Wall functions	HYDRA	**H-3DS-$k\varepsilon$-*WF***
		Resolved wall treatment	HYDRA	**H-3DS-$k\varepsilon$-*kl***
	SST k-ω model	Wall functions	FLUENT	**F-3DS-SST-*WF***
3D with extended inlet slot	Baseline k-ω (BSL)	Wall functions	CFX	**C-3DES-BSL-*WF***
		Resolved wall treatment		**C-3DES-BSL**
	SST k-ω	Wall functions	CFX	**C-3DES-SST-*WF***
		Resolved wall treatment		**C-3DES-SST**
3D with nozzle	Standard k-ε model	Wall functions	FLUENT	**F-3DN-$k\varepsilon$-*WF***

Table 2: Turbulence models used in the study.

imposing an inlet swirl angle, θ = 20 degrees or by specifying the swirl velocity for the extended slot geometry. Inlet turbulence conditions were specified assuming 5% turbulence intensity and a turbulence length scale of ~1 mm in all calculations. Dependency on the inlet turbulence conditions was also checked, and the results were not significantly affected. In this paper all walls were modelled with no-slip, no penetration boundary conditions. Except where otherwise stated, walls were assumed to be adiabatic.

Three different CFD solvers have been tested: FLUENT version 6.3.16, CFX version 11, and a modified version of Rolls-Royce's in-house code Hydra [27]. In FLUENT, the Reynolds-averaged Navier-Stokes and turbulence model equations were solved in a segregated manner using the SIMPLE (Semi Implicit Method for Pressure-Linked Equations) algorithm. In CFX and Hydra the equations were solved in a coupled manner using density-based algorithms. In all cases compressible flow was assumed using the ideal gas and Sutherland's laws for the density and viscosity of air, and including frictional effects in the energy equation.

All simulations presented here were carried out with second-order discretisation accuracy. Various convergence criteria were used. Residuals, as calculated in the different codes, reduced satisfactorily. Overall mass, angular momentum and energy balance errors were less than 1% of the inlet mass flow rate, change in angular momentum of the flow between inlet and exit, and change in total enthalpy of the flow between inlet and exit, respectively. Usually mass balance criteria were achieved within a few thousand iterations but many more

iterations were required to satisfy the momentum and energy balance criteria. To aid convergence some computations were started using first-order accurate discretisation, then switched to second order after a few hundred iterations.

The different models used are summarized in Table 2, which include a range of commonly available eddy viscosity turbulence models in combination with wall-function and resolved near-wall flow treatments. An Identifier (right-hand column) is given to all cases where calculations are shown in subsequent figures. This Identifier indicates the code used, the CFD geometry, and the turbulence model, and is used to label results presented below.

The FLUENT and Hydra simulations were performed on a PC cluster with 128 nodes (quad core, 2.6 GHz) and Myrinet networking at the University of Surrey. The CFX simulations were performed on 4 processors desktop PC at University of Bath. The mesh sizes for the axisymmetric model were in the range of 2000 (for wall function models) to 22,000 cells (for resolved wall models). The mesh sizes for the 3D model were 60,000 (for wall function models) to 2.5 million cells (for resolved wall models). For axisymmetric models, the computation time was within a few hours with one node; for the 3D cases, the computational time varied from 24 hours (with one node) for wall function models to about 5 days (with 16 nodes) for resolved wall models with the use of multiprocessors.

4 FLUID DYNAMICS

4.1 Axisymmetric model

For the axisymmetric case, eight different turbulence models (shown in Table 2) were tested in FLUENT, though the results from only five are shown here. The turbulence model comparison was carried out for λ_T = 0.127, 0.235 and 0.369, each at a rotational Reynolds number $Re_\phi = 0.78\times10^6$. Here, the results are presented for λ_T = 0.369 only, the condition which featured the strongest pre-swirl jet. Figure 3a shows the predictions of core swirl fraction ($v_\phi/\Omega r$) given by five turbulence models. These are compared with experimental velocities estimated from the measured static and total pressures shown in Figures 3b and 3c. It can be seen that the maximum value of swirl velocity occurs at the nozzle radius ($r/b \sim 0.74$) where there is consistency between experiment and all turbulence models. However all turbulence models fail to predict the constant core-swirl region (with $v_\phi/\Omega r \sim 0.6$) for $r/b > 0.85$. All turbulence models show similar trends for core swirl velocity but some variation is observed either side of the nozzle radius where the nozzle jet flow entrains the surrounding flow. None of the models captured the abrupt reduction in swirl velocity at $r/b \sim 0.81$ shown by the experimental data. This suggests that the either the axisymmetric slot is unable to appropriately model the pre-swirl jets, or the turbulence models are unable to appropriately cope with the complex flow in this region.

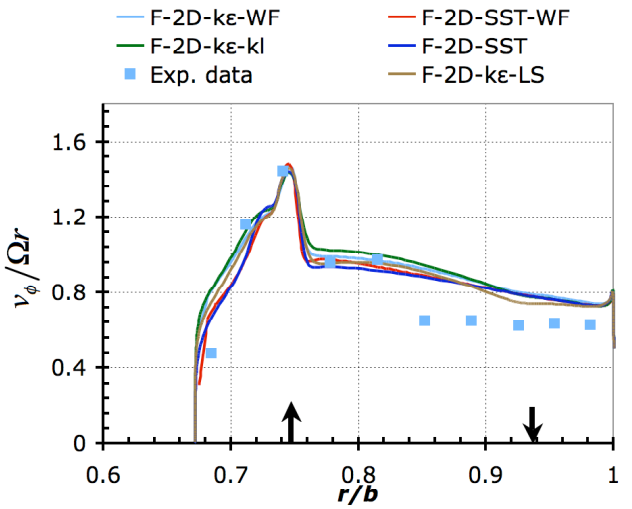

(a) Swirl velocity at z/s = 0.5

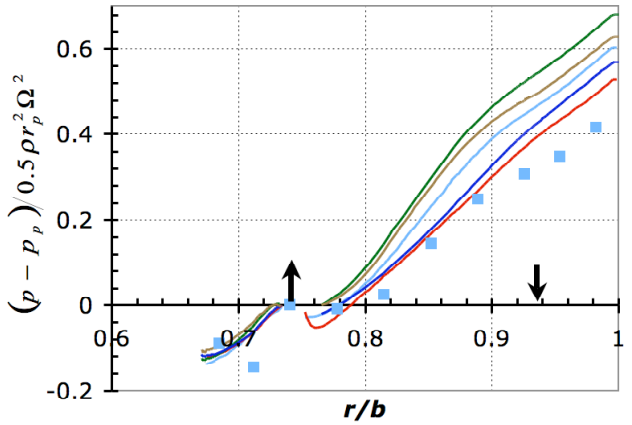

(b) Static pressure on the stator wall

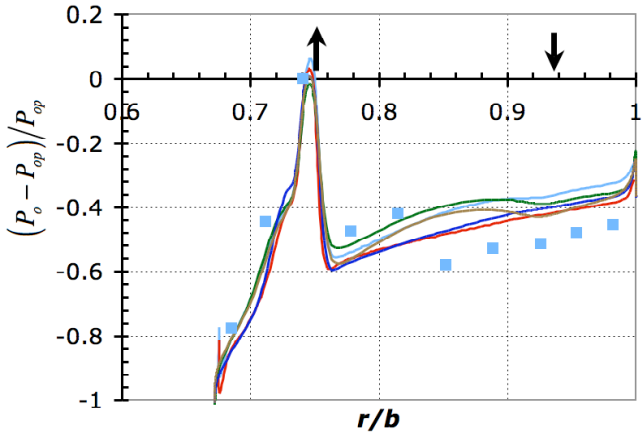

(c) Total pressure at z/s = 0.5

Fig. 3: Axisymmetric model results, λ_T =0.369, Re_ϕ = 0.78×10^6.

Figures 3b and 3c compare computed static and total pressures with experimental data on the stator wall and on the axial mid-plane of the cavity. In the non-dimensional static pressure calculation, p_p is taken at the lower edge of the inlet slot. In the non-dimensional total pressure calculation, P_{op} is a

gauge total pressure at the nozzle radius midway between rotor and stator. All models feature broad agreement and qualitatively capture the prominent features of the experiments. All models, however, over-predict the static pressure at outer radii, although the predicted gradients in this region show little variation between models and are similar to that measured by experiment. As found for the swirl velocity, the non-dimensional total pressure is well predicted at low radius near the pre-swirl nozzles but does not capture the abrupt reduction at $r/b \sim 0.81$ shown by the experimental data. This again suggests that the losses associated with the jet mixing at lower radii are not predicted well. However it may be noted that the different turbulence models predict significantly different total pressure losses.

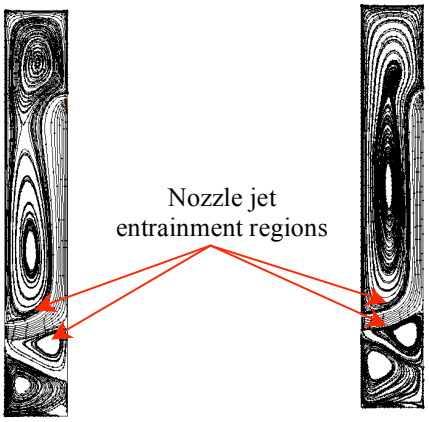

(a) F-2D-kε-kl b) F-2D-SST

Fig. 4: Pathlines from axisymmetric models, λ_T=0.369.

Figure 4 shows flow pathlines for the *k-ε* and *k-ω* turbulence models. It can be seen that the models predict different vortex structures at higher radii. All the results, apart from those of the RNG *k-ε* and *k-ω* models, showed similar flow patterns to Figure 4a. All the *k-ω* model results at high flow rates fitted the flow pattern in Figure 4b. With a different flow pattern at higher radii, the *k-ω* model predicts lower pressure than the *k-ε* model. At a lower flow rate, $\lambda_T = 0.127$, the vortex structures given by all turbulence models were similar to that in Figure 4a.

Angular moment coefficients ($C_m = M/0.5\rho\Omega^2 b^5$) for the stator and rotor walls were calculated in all cases studied. For the three conditions considered, these agreed within 10% for all turbulence models except the Launder-Sharma low-Reynolds number; this model gave significantly higher moments. Indeed, the RNG *k-ε* model and the Launder-Sharma low-Reynolds number *k-ε* model showed some discouraging results and were not used further.

Considering its geometric limitations, the overall performance of the axisymmetric model might be considered acceptable for most of the turbulence models used and the results encouraging. To improve the jet-mixing predictions at low radius it may be necessary to model the pre-swirl jets. Similarly, discrete receiver holes should improve the modelling in the outer part of the cavity. Hence 3D steady state calculations were undertaken in the next stage of the research and are reported below.

4.2 3D sector models

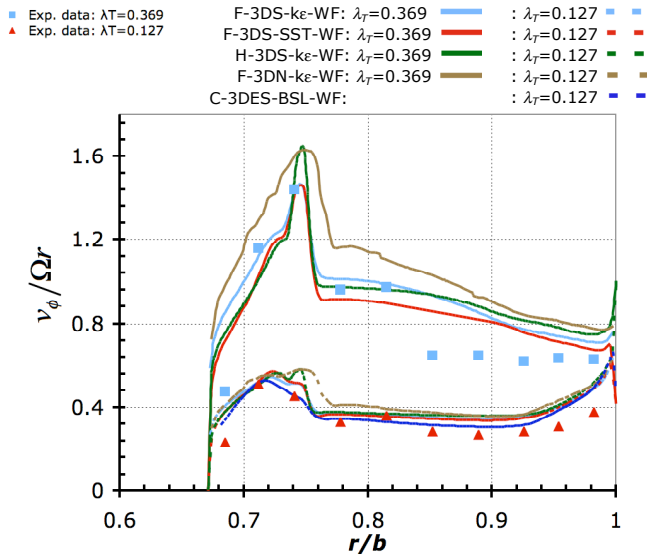

(a) Swirl velocity at $z/s = 0.5$

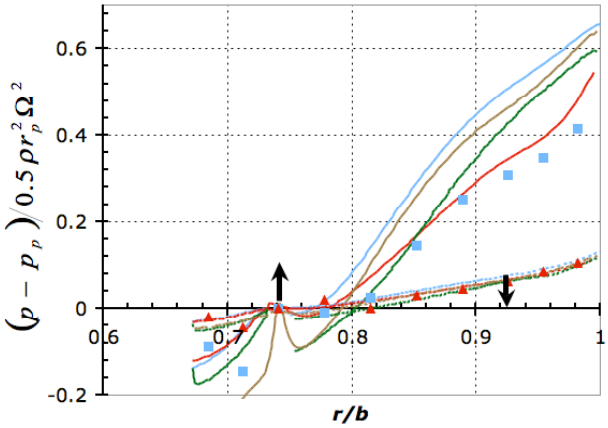

(b) Static pressure on the stator wall

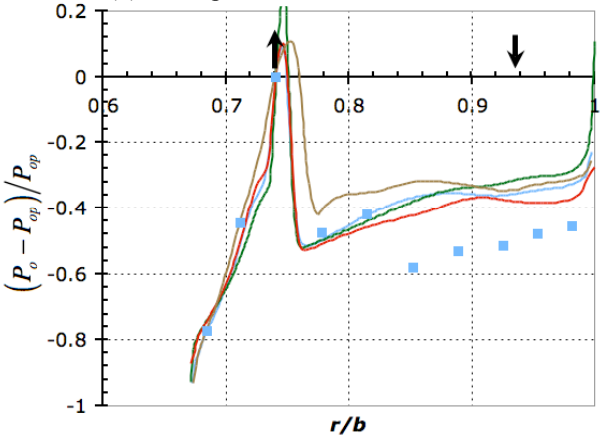

(c) Total pressure at $z/s = 0.5$

Fig. 5: 3D model results.

For the 3D sector models, three CFD codes have been tested: FLUENT, CFX and Hydra. Results are presented for two operating conditions: λ_T = 0.123 and 0.369. Apart from one case, $Re_\phi = 0.78\times10^6$; the exceptional case is C-3DES-BSL-WF, for which $Re_\phi = 1.2\times10^6$.

At the low flow rate, $\lambda_T = 0.123$, shown in Figures 5a and 5b only, there is reasonable agreement of predictions and experiment. For λ_T = 0.369, none of the more detailed 3D models improved the comparison with the experimental data. Preliminary studies using Reynolds stress modelling for steady flow and full-unsteady *k-ε* model simulations including both nozzles and receiver holes (not presented here) have produced similar results to the steady 3D simulations. This similarity reinforces the suggestion that there are deficiencies in the turbulence modelling. An improved simulation may be obtained with large eddy simulations, which include the calculation of large turbulence structures and this is an area for future research.

As in the axisymmetric case, some variation between results from the different turbulence models is found, but ranking the turbulence models on these results alone could be misleading. Differences between the results produced by FLUENT and Hydra are attributed to different implementations of the wall functions.

Overall, the fluid-dynamics results are encouraging for the use of CFD in pre-swirl-system design. The different codes and most turbulence models have shown broad agreement and have captured most of the prominent features of the experiments. The more detailed 3D modelling did not significantly improve the comparison with experiment and the deficiencies in the turbulence models could suggest difficulties for the CFD in accurately predicting the convective heat transfer in these systems.

5 HEAT TRANSFER

To calculate heat transfer on the rotor disc, a constant temperature (20° C) boundary condition was applied on the rotor walls in all models. Comparisons are made with measurements presented by Kakade *et al.* [20]. Heat transfer results are presented in the form of a local Nusselt number (*Nu*) on the rotor defined as follows:

$$Nu = \frac{hr}{k_a} \qquad h = \frac{q_w}{T_w - T_{w,ad}} \tag{1}$$

Here h is the convective heat transfer coefficient, k_a is thermal conductivity of air, q_w is wall heat flux, T_w is wall temperature, and $T_{w,ad}$ is an adiabatic wall temperature given by the following equation [23]:

$$T_{w,ad} = T_{0,p} - \frac{v_\phi^2}{2C_p} + \mathrm{Pr}^{1/3}\frac{\Omega^2 r^2}{2C_p}\left(1 - \frac{v_\phi}{\Omega r}\right)^2 \tag{2}$$

Here $T_{0,p}$, C_p and Pr denote air inlet total temperature, specific heat and Prandtl number. For fully turbulent flow dominated by rotational effects, it is expected that $Nu\mathrm{Re}_\phi^{-0.8}$ will be approximately independent of Re_ϕ, if λ_T and SR_p are unchanged.

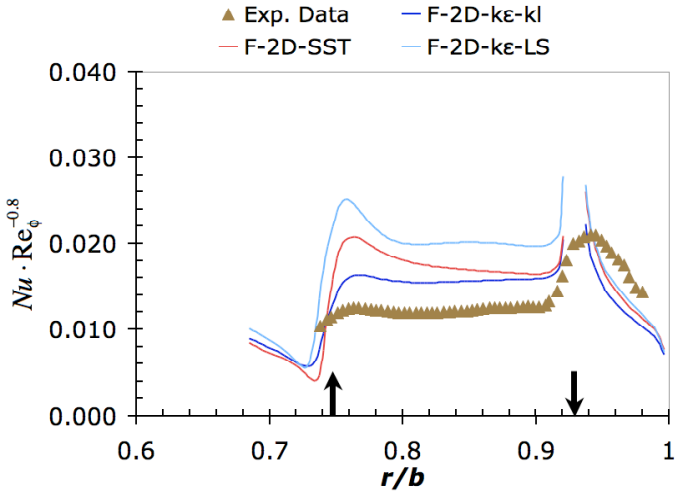

(a) $\lambda_T = 0.127$, $SR_p = 0.52$

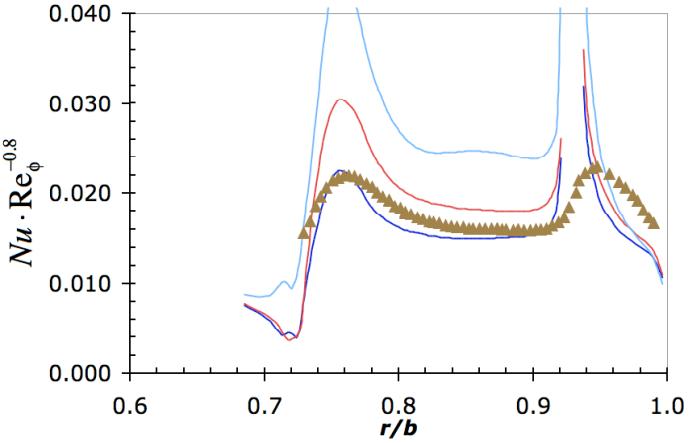

(b) $\lambda_T = 0.235$, $SR_p = 0.95$

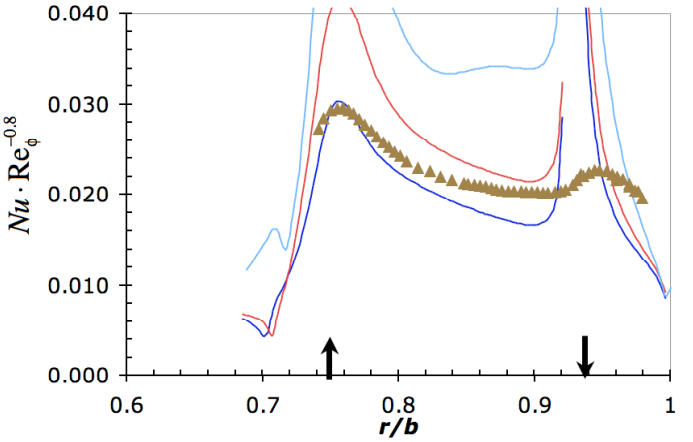

(c) $\lambda_T = 0.369$, $SR_p = 1.49$

Fig. 6: Axisymmetric model heat transfer results, $Re_\phi = 0.78\times10^6$.

5.1 Axisymmetric models

Figure 6 shows the variation of $Nu\mathrm{Re}_\phi^{-0.8}$ with non-dimensional radius as determined by different turbulence models and by experiment. The CFD predictions are axisymmetric while the experiments are 3D and this data is shown along a line midway between two receiver holes. The heat-transfer peak at the pre-swirl nozzle is due to impingement and is observed to increase with increasing λ_T and SR_p. The peak at the receiver-hole radius is associated with a region where thin boundary layers replace air exiting though holes on the rotating disc [20].

CFD results are shown for three turbulence models, each of which resolve the near-wall flow region. For the three flow conditions all turbulence models qualitatively predict the shape of experimental data very well. The only exception is at the receiver-hole radius where the axisymmetric slot cannot simulate the local flow features, which dominate in the experimental configuration.

At all flow conditions the two-layer *k-ε/k-l* model performs better, providing very good quantitative agreement with experiment at the higher flow rates ($\lambda_T = 0.369$ and $\lambda_T = 0.235$). At the lowest flow rate ($\lambda_T = 0.127$) the model over-predicts the heat transfer. The Launder-Sharma low-Reynolds number model gives marked over-predictions for all three flow rates. The SST *k-ω* model consistently over-predicts the heat transfer in the impingement region at the pre-swirl radius and consistently falls between the low Re and *k-ε/k-l* models.

Note that for the fluid dynamics results (shown in Figure 3) the SST *k-ω* model, not the *k-ε/k-l* model, provided closer agreement to the experimental data. Also the fluid-dynamic predictions were better at the lowest flow rate.

All models over-predict heat transfer for $\lambda_T = 0.127$. It may be conjectured that is associated with low Reynolds number effects in the experiment: if the experimental flow is not fully turbulent then low-Re effects may be stronger at low flow rates with weaker pre-swirl jets. However, the scaling of *Nu* with $\mathrm{Re}^{0.8}$ identified by Kakade *et al.* [20] suggests turbulent flow.

5.2 3D models

Figures 7 and 8 show the variation of $Nu\mathrm{Re}_\phi^{-0.8}$ with non-dimensional radius as determined by different turbulence models and by experiment. All calculations are from models with an inlet slot and results are shown along a line midway between two receiver holes. Results are shown for two different Reynolds numbers and two flow rates, $\lambda_T = 0.127$ and $\lambda_T = 0.369$.

Figure 7 presents calculations from models using wall functions and Figure 8 from models with resolved wall layer treatments. As for the axisymmetric model, fair agreement between CFD and measurements is shown at the higher flow rate ($\lambda_T = 0.369$) and lower Reynolds number ($\mathrm{Re}_\phi = 0.78\times10^6$). At this condition Hydra predicts high heat transfer in the impingement region when employing wall functions but agrees reasonably well with FLUENT when using the two layer *k-ε/k-l* model. In Figure 7, the differences in heat transfer prediction from different codes are associated with different implementation of wall functions and numerical techniques in the different codes. In Figure 8, all three codes gave quite similar results for resolved wall turbulence models.

Results for $\lambda_T = 0.369$, $\mathrm{Re}_\phi = 1.2\times10^6$ in Figure 7b indicate overprediction of heat transfer by the CFD. There is clearly some difference between CFD and experimental results for the scaling of *Nu* with Re_ϕ for this value of λ_T.

As for the axisymmetric model, over-prediction of heat transfer is observed for $\lambda_T = 0.127$. The trends from the axisymmetric and 3D models are broadly similar apart from the region near the receiver-hole radius.

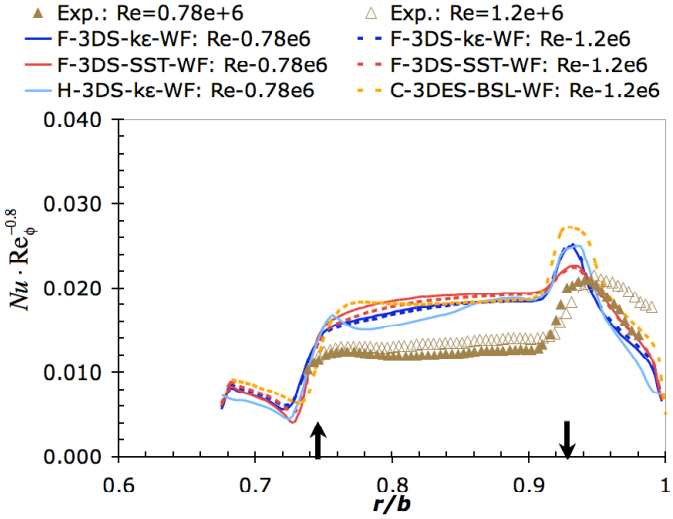

(a) $\lambda_T = 0.127$, $SR_p = 0.52$ at $\mathrm{Re}_\phi = 0.78\times10^6$ and $\lambda_T = 0.13$, $SR_p = 0.48$ at $\mathrm{Re}_\phi = 1.2\times10^6$

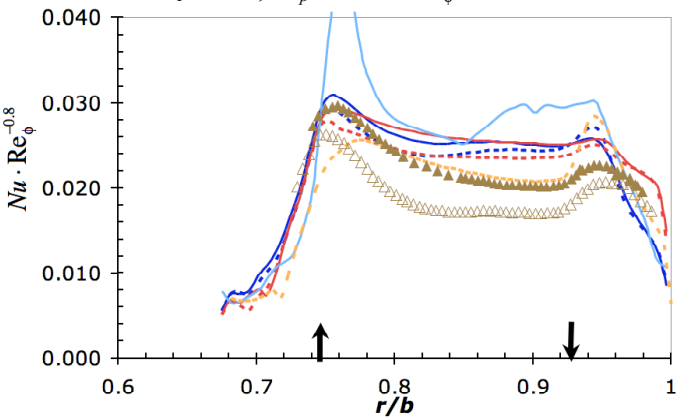

(b) $\lambda_T = 0.369$, $SR_p = 1.49$ at $\mathrm{Re}_\phi = 0.78\times10^6$ and $\lambda_T = 0.37$, $SR_p = 1.41$ at $\mathrm{Re}_\phi = 1.2\times10^6$

Fig. 7: Heat transfer results from 3D models with wall functions.

The prominent differences between predictions shown in Figures 7 (wall functions) and 8 (resolved layer) occur near the impingement region at the pre-swirl radius and in the region near the receiver-hole radius. In the impingement region, the wall function treatment dominates over the details of the different turbulence modelling and provides calculations closer

to the experimental peak. The wall function treatment also provides superior predictions at the receiver-hole radius. At the low flow rate (λ_T = 0.127) the resolved near-wall treatments produce a twin peak that has not been observed experimentally. Further investigation revealed that this was due to a small region of reverse flow computed near the edge of the receiver hole (*i.e.* axial flow into the wheel-space from the receiver hole).This phenomenon was not observed when using the wall function-based models.

Away from the receiver holes the results from the different turbulence models are generally consistent, regardless of whether the wall-function or two-layer treatment is used. The one exception is the calculation from Hydra in Figure 7b discussed above. At the lower flow rate the heat transfer from Hydra agrees reasonably well with that from FLUENT and CFX.

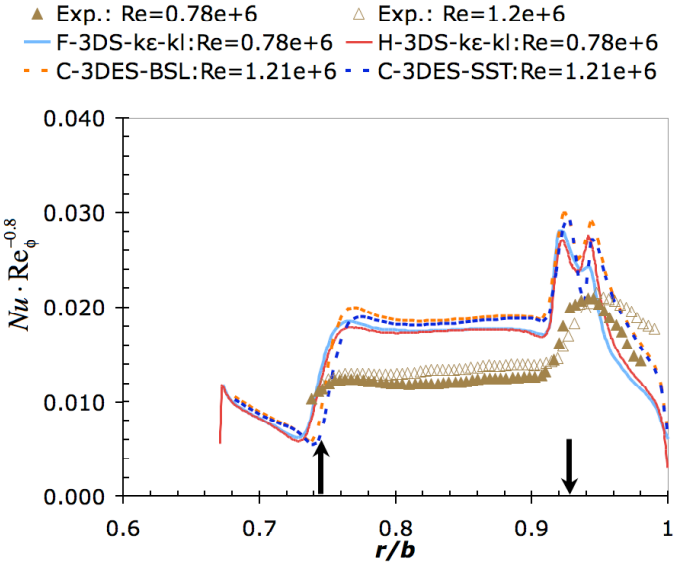

(a) λ_T = 0.127, SR_p = 0.52 at Re_ϕ = 0.78×10^6 and λ_T = 0.13, SR_p = 0.48 at Re_ϕ = 1.2×10^6

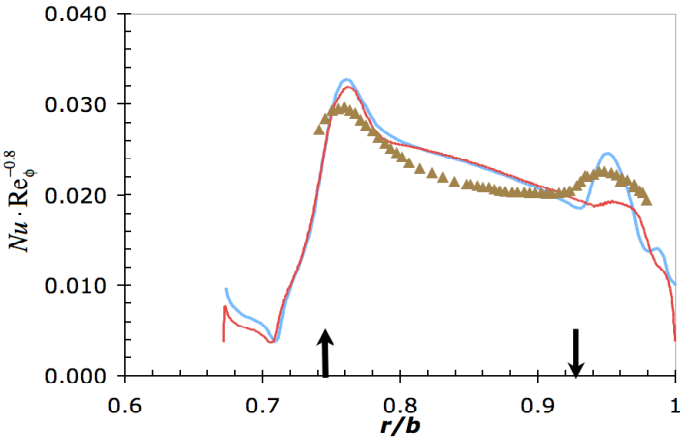

(b) λ_T = 0.369, SR_p = 1.49 at Re_ϕ = 0.78×10^6

Fig. 8: Heat transfer results from 3D models with resolved wall layer treatments.

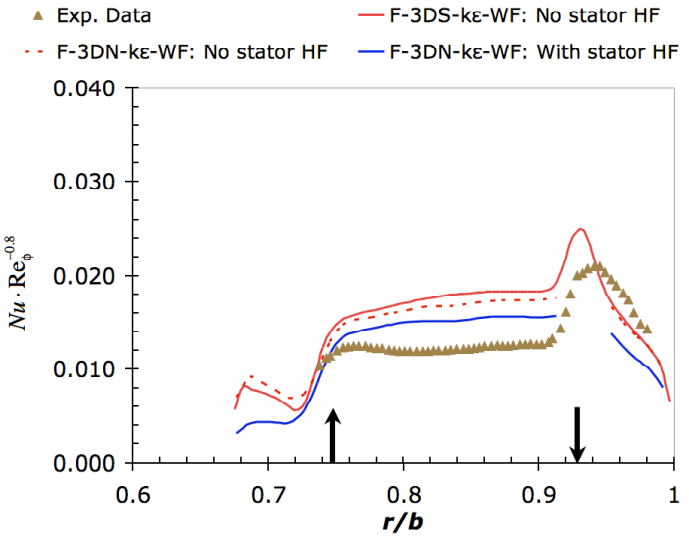

(a) λ_T=0.127, SR_p= 0.52

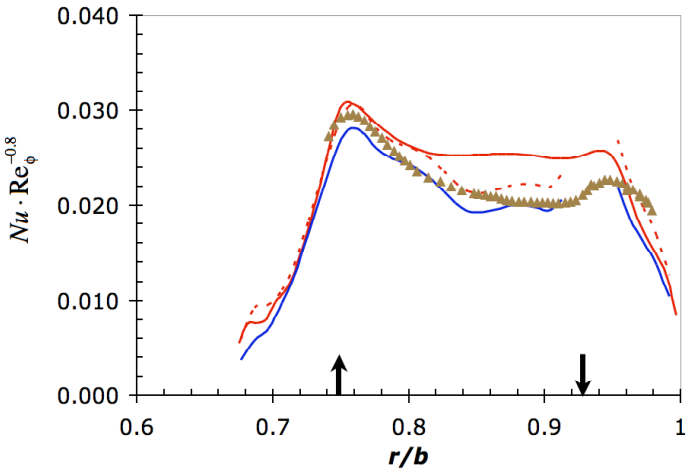

(b) λ_T=0.369, SR_p= 1.49

Fig. 9: Heat transfer results from 3D models showing effects of including nozzles and stator disc heat transfer, Re_ϕ=0.78×10^6.

The experiment was transient with the rotor and stator temperatures varying between approximately 20 and 60° C. The influence of heat transfer to the stator (which was thermally insulated using polycarbonate) is thought to be small as the heat transfer measured at two different rotor wall temperatures (30 and 40° C) was equal within experimental uncertainty [20]. However, in order to bound the issue of stator heat transfer, calculations have been conducted with the stator at the same temperature as the unheated rotor (*i.e.* 20°C) rather than using an adiabatic boundary condition at this surface. The calculations were conducted at both flow rates and using a 3D model of the pre-swirl nozzle which had the potential advantage of better modelling the inlet jet structure. Figure 9 shows the effects of including the 3D nozzle model and of the thermal boundary condition on the stator. These bring the CFD results closer to the measurements for both values of λ_T considered. Nevertheless, for λ_T =0.127, the influence of stator

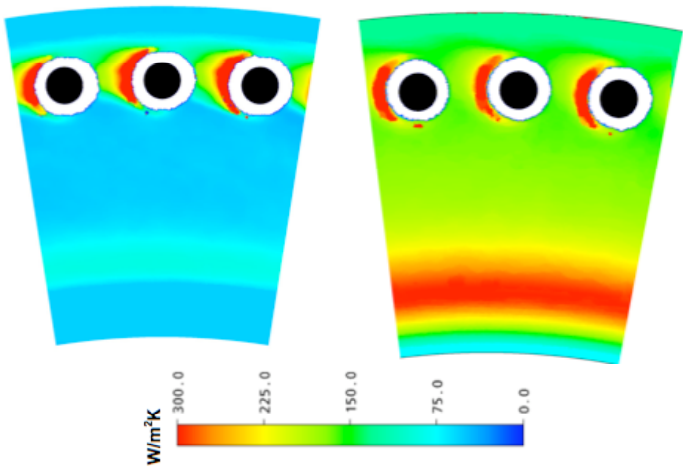

Left: λ_T=0.123 Right: λ_T=0.353

(a) Experimental data, $Re_\phi=0.97\times10^6$

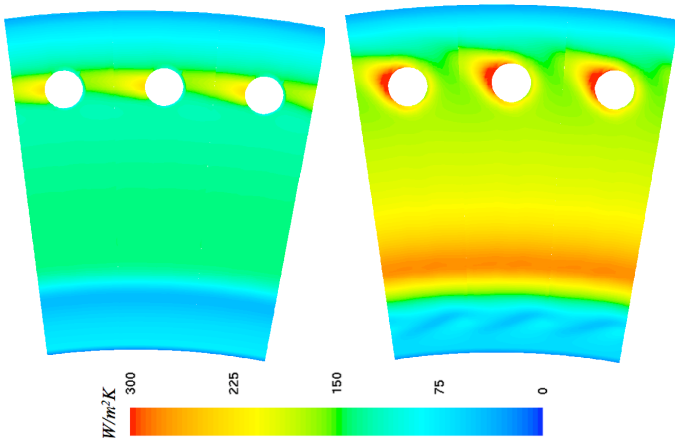

Left: λ_T=0.127 Right: λ_T=0.369

(b) F-3DS-$k\varepsilon$-WF, $Re_\phi=0.78\times10^6$

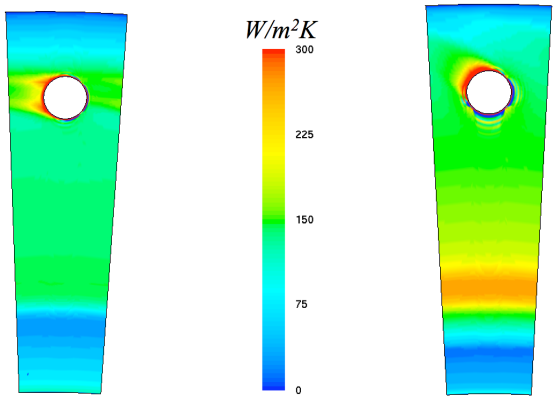

Left: λ_T=0.127 Right: λ_T=0.369

(c) H-3DS-$k\varepsilon$-kl, Re_ϕ= 0.78×10^6

Fig. 10: Contour plots of heat transfer coefficient on the rotor. The disc is rotating clockwise.

heat transfer does not fully address the over-prediction at all radii.

In Figure 9b the model including the nozzle shows closer agreement with measurements than the model including the receiver holes. However, it is not clear whether this is due to inclusion of the nozzles or replacement of the receiver holes with a slot boundary condition. Comparison of the axisymmetric model results with the 3D models confirms that the treatment of the receiver holes can affect the heat transfer at lower radii. This might be expected considering the recirculating flow shown in Figure 4.

5.3 Heat transfer near the receiver holes

Examples of calculated and measured local heat transfer coefficient contour plots on the rotor disc are shown in Figure 10 (disc rotating clock-wise). Note that the experiments are at slightly higher Reynolds number than the computations, and that no experimental results are available immediately around the receiver holes owing to the use of insulating material here.

Similar trends are apparent to those in the line plots above. However, the contours reveal high levels of h on the downstream side of the receiver holes where three-dimensional flow near the surface of the disc creates a non-axisymmetric distribution of heat transfer; here the disc is exposed to impingement, the boundary layer flow having been sucked into the receiver hole. Figure 10c shows a "double lobed" feature downstream of the holes, corresponding to the double peak in the line plots noted above. There is some difference between results from different turbulence models in this region and with experiments. This is perhaps to be expected as this complex flow will be challenging for the turbulence models. Close to the receiver holes the near wall resolved models depart further from the experiment than the wall function models.

Overall comparison with heat transfer results showed qualitative agreement but the quantitative agreement is poor for some cases. Nevertheless it is considered that CFD can give useful estimates of heat transfer in direct transfer preswirl systems but further investigations would clearly be beneficial.

6 CONCLUSIONS

Detailed evaluations of steady CFD models using eddy viscosity turbulent models have been undertaken through comparison with flow and heat transfer measurements in a pre-swirl chamber. The results are generally considered encouraging for use of CFD in design calculations, although some care and caution is required.

A number of commonly used turbulence models were tested. The RNG k-ε model and the Launder-Sharma low-Reynolds number k-ε model showed some discouraging results in initial 2D evaluations and were not used further. Other models and the three CFD codes used can all be said to have given reasonable results, showing broad agreement and capturing many features of the experiments. None of the models capture the full details of the flow in the cavity near the pre-swirl jets, and appear to underpredict total pressure losses in this region. This is attributed to turbulence model limitations in complex flows. Near the receiver holes there is some

qualitative agreement between CFD and measured disc heat transfer. The CFD results are sensitive to near-wall turbulence modelling in this region. Elsewhere models resolving the near wall flow and those using wall functions generally showed fair agreement. Close to the receiver holes the near-wall resolved models departed further from the experiment than the wall function models.

In one of the CFD codes heat transfer in the jet impingement region was rather high when wall functions were used. This shows some sensitivity to how wall functions are implemented in regions where their validity is questionable.

Heat transfer over the main part of the rotating disc was reasonably well predicted by CFD at the two higher flow rates and swirl rates considered for $Re_\phi=0.78\times10^6$. At the lowest flow rate considered, CFD significantly over-predicted the heat transfer. There is some indication from consideration of the conditions that this could be due to low Reynolds effects, but Reynolds number scaling observed in the experiments suggests fully turbulent flow. Sensitivity to heat transfer on the stator, which is somewhat uncertain in the experiment, may account for some of the over-prediction of rotor heat transfer by CFD, but this has not been fully explained. Some discrepancies between CFD and measurement have also been noted for the highest flow rate and considered with $Re_\phi=1.2\times10^6$. Again this is not fully understood, and there is clearly scope for further detailed investigation. Eddy viscosity models are commonly used to predict the flow in internal air systems, and with notable success. However, for the cases studied here, these models show some limitations.

Considering the overall results, it is concluded that steady RANS models can provide useful estimates of the detailed flow and heat transfer in pre-swirl systems, but that care is needed in modelling choices and interpretation of results. Given the complex fluid dynamics involved, the eddy viscosity turbulence models considered here are expected to have limitations and these have been illustrated here. Further research to evaluate unsteady effects, and large-eddy simulation to improve modelling of the pre-swirl jet region is needed, although application of such methods in design is currently limited by high computing requirements.

ACKNOWLEDGMENTS

The authors are grateful to the EPSRC, China Scholarship Council and Rolls-Royce for financial support of this work, and to colleagues for helpful comments. Particular thanks are extended to Dr Tim Scanlon at Rolls-Royce, Derby. The authors gratefully acknowledge the permission of Rolls-Royce plc to publish this paper.

REFERENCES

1. Meierhofer B., and Franklin C. J., “An Investigation of a preswirled cooling airflow to a turbine disc by measuring the air temperature in the rotating channels”, ASME Paper 81-GT-132, 1981.
2. Smout P. D., “ICAS-GT-EU research into gas turbine internal air system performance”, Air & Space Europe, vol. 3, issues 3-4, pp. 166-169, 2001.
3. Dittmann M., Geis T., Schramm V., Kim, S., and Wittig, S., “Discharge coefficients of a preswirl system in secondary air systems”, ASME Journal of Turbomachinery, vol. 124, pp. 119–124, 2002.
4. Geis T., Rottenkolber G., Dittmann M., Richter B., Dullenkopf K., and Wittig S., “Endoscopic PIV-measurements in an enclosed rotor-stator system with pre-swirled cooling air”, Proceedings of the 11th International symposium on application of laser techniques to fluid mechanics, Lisbon, Portugal, July 2002.
5. Bricaud C. Dullenkopf K. and Bauer H. J., “Heat Transfer Measurements at the rotor disc of a direct transfer preswirl system”, 17th International Symposium on Airbreathing Engines ISABE-1073, 2005.
6. Geis T., Dittmann M., and Dullenkopf K., “Cooling air temperature reduction in a direct transfer preswirl system”, ASME Paper GT2003-38231, 2003.
7. Bricaud C. Dullenkopf K., Bauer H. J. and Geis T., “Measurement and analysis of aerodynamic and thermodynamic losses in preswirl system arrangements”, ASME Paper GT-2007-27191, 2007.
8. Benim A.C. Bonhoff B. Bricaud C. Brillert D., and Cagan M., “Computational analysis of flow and heat transfer in a direct transfer pre-swirl system”, 6th European Conference on Turbomachinery, Lille, France, 2005.
9. Benim A.C., Brillert D. and Cagan M., "Investigation into the computational analysis of direct transfer preswirl systems for gas turbine cooling”, ASME Paper GT-2004-54151, 2004.
10. Chew J. W., Ciampoli F., Hills N. J., and Scanlon, T., “Pre-swirled cooling air delivery system performance”, ASME Paper GT2005-68323, 2005.
11. Ciampoli F., Hills N. J., Chew J. W., and Scanlon, T., “Unsteady numerical simulation of the flow in a direct transfer preswirl system”, ASME Paper GT-2008-51198, 2008.
12. El-Oun Z. B. and Owen, J. M., “Preswirl Blade-Cooling Effectiveness in an adiabatic rotor-stator System”, ASME Journal of Turbomachinery, vol. 124, pp. 522–529, 1989.
13. Chew J. W., Hills N. J., Khalatov S., Scanlon T. and Turner A. B., “Measurements and analysis of flow in a preswirled cooling air delivery system”, Proceedings of ASME Paper GT-2003-38084, 2003.
14. Wilson M., Pilbrow R. and Owen J. M., “Flow and heat transfer in a pre-swirl rotor-stator system”, ASME Journal of Turbomachinery, vol. 119, pp. 364 –373, 1997.

15. Karabay H., Chen J. X., Pilbrow R., Wilson M. and Owen J.M., “Flow in a “Cover-plate” preswirl rotor-stator system”, ASME Journal of Turbomachinery, vol. 121, pp. 160-166, 1999.

16. Yan Y., Farzaneh-Gord M., Lock G., Wilson M., and Owen J. M., “Fluid dynamics of a preswirl rotor-stator system”, ASME Journal of Turbomachinery, vol. 125, pp. 641–647, 2003.

17. Farzaneh-Gord M., Wilson M., and Owen J. M., “Numerical and theoretical study of flow and heat transfer in a preswirl rotor-stator system”, ASME Turbo Expo: Power for Land, Sea and Air, Reno-Tahoe, USA, GT2005-68135, 2005.

18. Lewis P., Wilson M., Lock G. D. and Owen J. M., “Physical interpretation of flow and heat transfer in preswirl systems”, J. of Engineering for Gas Turbines and Power, vol. 129, pp. 769-777, 2007.

19. Lock G. D., Wilson M., and Owen J. M., “Influence of fluid dynamics on heat transfer in a pre-swirl rotating disc system”, ASME Journal of Engineering for Gas Turbines and Power, vol. 127, pp. 791–797, 2005.

20. Kakade V. U., Lock G. D., Wilson M., Owen J. M. and Mayhew, J. E., “ Effects of radial location of nozzles on heat transfer in preswirl cooling systems”, ASME Paper GT2009-59090, 2009.

21. Lewis P., Wilson M., Lock G. D. and Owen J. M., 2009. "Effect of radial location of nozzles on performance of pre-swirl systems," IMechE Part A, Journal of Power and Energy, (223) 2, pp 179-190.

22. Kakade V. U., Lock G. D., Wilson M., Owen J. M. and Mayhew J. E., "Accurate heat transfer measurements using thermochromic liquid crystals. Part 2: application to rotating disc", International Journal of Heat and Fluid Flow, vol. 30, pp 950-959, 2009.

23. Newton P. J., Yan Y., Stevens N. E., Evatt S. T., Lock G.D. and Owen J. M., 2003. "Transient heat transfer measurements using thermochromic liquid crystal. Part 1: An improved technique", International Journal of Heat Fluid Flow, vol. 24, pp. 14-22, 2003.

24. Kakade V. U., Lock G. D., Wilson M., Owen J. M. and Mayhew J. E., "Accurate heat transfer measurements using thermochromic liquid crystals. Part 1: Calibration and characteristics of crystals" International Journal of Heat and Fluid Flow, vol. 30, pp 939-949, 2009.

25. Owen J. M., Newton P. J. and Lock G. D., "Transient heat transfer measurements using thermochromic liquid crystal. Part 2: Experimental uncertainties", International Journal of Heat and Fluid Flow, vol. 24, pp. 23-28, 2003.

26. Kingsley-Rowe J. R., Lock G. D. and Owen J. M., "Transient heat transfer measurements using thermochromic liquid crystal: Lateral-conduction error", International Journal of Heat and Fluid Flow, vol. 26, pp. 256-263, 2005.

27. Lapworth, L., “Hydra-CFD: a framework for collaborative CFD development”, International Conference on Scientific and Engineering Computation (IC-SEC), 2004.